HHS Public Access

Author manuscript

Photodiagnosis Photodyn Ther. Author manuscript; available in PMC 2015 June 16.

Published in final edited form as:

Photodiagnosis Photodyn Ther. 2006 December ; 3(4): 234–246. doi:10.1016/j.pdpdt.2006.08.002.

Prostate PDT dosimetry

Timothy C. Zhu, PhD[*] and **Jarod C. Finlay**

Department of Radiation Oncology, University of Pennsylvania, 3400 Spruce Street/2 Doner Bldg., Philadelphia, PA 19104, USA

Summary

We provide a review of the current state of dosimetry in prostate photodynamic therapy (PDT). PDT of the human prostate has been performed with a number of different photosensitizers and with a variety of dosimetry schemes. The simplest clinical light dose prescription is to quantify the total light energy emitted per length (J/cm) of cylindrical diffusing fibers (CDF) for patients treated with a defined photosensitizer injection per body weight. However, this approach does not take into account the light scattering by tissue and usually underestimates the local light fluence rate, and consequently the fluence. Techniques have been developed to characterize tissue optical properties and light fluence rates *in vivo* using interstitial measurements during prostate PDT. Optical methods have been developed to characterize tissue absorption and scattering spectra, which in turn provide information about tissue oxygenation and drug concentration. Fluorescence techniques can be used to quantify drug concentrations and photobleaching rates of photosensitizers.

Keywords

Prostate PDT dosimetry; *In vivo*; Optical properties; Photosensitizer concentration; Light fluence rate; Cimmino feasibility algorithm; Combinatorial search; Optimization

Introduction

Prostate adenocarcinoma is the most common malignancy in men. In 2006 an estimated 234,460 cases of prostate adenocarcinoma will be diagnosed in the United States [1]. Although the availability of serum prostate-specific antigen (PSA) measurement as a screening tool has resulted in earlier detection of the disease [2], prostate cancer still accounts for 27,350 deaths per year [1]. The conventional treatment options for early stage prostate cancer include radical prostatectomy, radiation therapy (either external beam or radioactive seed implantation) and hormonal therapy.

Photodynamic therapy (PDT) is an emerging cancer treatment modality based on the interaction of light, a photosensitizing drug, and oxygen [3]. PDT has been approved by the US Food and Drug Administration for the treatment of microinvasive lung cancer, obstructing lung cancer, and obstructing esophageal cancer and Barrett's esophagus with

[*]Corresponding author. Tel.: +1 215 662 4043; fax: +1 215 349 5978. tzhu@mail.med.upenn.edu (T.C. Zhu).

high grade dysplasia. The prostate is a good target organ for PDT because prostate cancers are often locally confined and techniques already exist for the interstitial administration of radiation that are easily adapted. PDT could provide a second chance for cure in cases of locally recurrent prostate cancer after prior radiation therapy in which salvage options are limited [4].

Several PDT clinical trials on human prostate have been reported. A trial of interstitial prostate PDT in humans has been reported by Nathan et al. using meso-tetrahydroxyphenyl chlorin (mTHPC)-mediated PDT [5]. Zaak et al. reported preliminary results for ALA-mediated PDT of prostate cancer [6]. These early studies established significant changes of PSA after PDT. Current Phase I trials using motexafin lutetium (MLu) and Tookad utilize multiple interstitial linear fibers for ablation of the entire prostate gland [7–10]. Although all these studies are restricted to early stage clinical trials, it is imminent that a safe and effect PDT treatment will be developed for prostate cancer [11].

There has been tremendous progress in photodynamic therapy dosimetry since the early 1990s. Several preclinical studies have shown that PDT is a feasible treatment for prostate gland [12–20]. Clinical studies followed shortly thereafter [5,7–10]. The simplest clinical dose prescription for interstitial PDT is to quantify the total light energy emitted per length (J/cm) of the cylindrically diffusing fiber (CDF) for patients treated with a defined photosensitizer injection per body weight. However, this approach does not take into account the light scattering by tissue and usually underestimates the local light fluence rate, and consequently the fluence. Techniques have been developed to characterize the tissue optical properties and the light fluence rate *in vivo* [21,22]. Other optical spectroscopic methods [23,24] have been developed to characterize tissue absorption and scattering spectra, which in term provide information about tissue oxygenation and drug concentration. Fluorescence techniques [25,26] can be used to quantify drug concentration and can provide valuable dynamic information relating to the photobleaching of the photosensitizer and oxygen consumption.

The objective of this paper is to present a brief review of the issues related to the dosimetry of photodynamic therapy in the human prostate. In particular, we review the current start of art of techniques to quantify light fluence, drug concentration, tissue oxygenation, and PDT efficiency for prostate PDT.

Mechanism of photodynamic interaction

The photochemical reactions that result in photodynamic damage can be characterized as either Type I or Type II reactions. In Type I reactions, the photosensitizer in its excited state reacts directly with a substrate present in the tissue, leading to the generation of cytotoxic free radicals [27,28]. The majority of photosensitizers available for PDT utilize Type II photodynamic processes, i.e., the photodynamic effect is through the production of singlet oxygen [28,29]. The energy level diagram shown in Fig. 1 summarizes the underlying physical processes involved in Type-II PDT. The process begins with the absorption of a photon by photosensitizer in its singlet ground state (with a spin multiplicity of 1), promoting it to a singlet excited state. The photosensitizer molecule can return to its ground

state by emission of a fluorescence photon or by conversion to a triplet state (with a spin multiplicity of 3), a process known as intersystem crossing (ISC). Collisions between triplet photosensitizer and molecular oxygen produce highly reactive singlet oxygen ($^1O_2$) and return the photosensitizer to its ground state. Since the photosensitizer is not consumed in this process, the same photosensitizer molecule may create many singlet oxygen molecules. Once $^1O_2$ is created, it reacts almost immediately with cellular targets in its immediate vicinity. The majorities of these reactions are irreversible, and lead to consumption of oxygen. This consumption of oxygen can cause measurable decreases in tissue oxygenation when the incident light intensity is high enough. A small fraction of the singlet oxygen produced may return to its ground state via emission of a phosphorescence photon, which can be detected optically [30,31].

In addition to its reactions with cellular targets, singlet oxygen may react with the photosensitizer itself. This leads to its irreversible destruction (photobleaching), which decrease the effectiveness of PDT by reducing the photosensitizer concentration [32,33]. It can be used for dosimetry, as it is related directly to the reaction of $^1O_2$ [34–36].

Fundamentals of PDT dosimetry

To quantify the complex photodynamic effect, a dosimetric parameter called the “photodynamic dose” (PDT dose) has been introduced [37]. PDT dose is defined as the number of photons absorbed by photosensitizing drug per gram of tissue [ph/g] [37]. When the photobleaching of the photosensitizer during treatment is taken into account, PDT dose can be defined as follows:

$$D=\int_0^t \varepsilon c \times \frac{\phi(t')}{h\nu} \times \frac{1}{\rho} \mathrm{d}t', \quad (1)$$

where ρ is the density of tissue [g/cm^3], φ is the light fluence rate [W/cm^2], $h\nu$ is the energy of a photon [J/ph], c is the drug concentration in tissue [μM], ε is the extinction coefficient of the photosensitizer [1/cm/μM]. The logic in this choice is that light fluence rate (φ), drug concentration (c), and exposure time (t) are parameters under clinical control. For simplicity, we use the light fluence (fluence rate×exposure time, $\varphi \times t$) for the PDT dose throughout the paper, assuming uniform drug concentration.

The photodynamic dose (D) does not consider the quantum yield (η) of oxidative radicals, the effect of tissue oxygenation on η, or the fraction (f) of radicals that oxidize critical sites. The production of oxidative radicals which are capable of damaging the tissue can be expressed as [38]:

$$[^1O_2]_{rx} = f \times \eta \times D, \quad (3)$$

where f depends on the localization of the photosensitizer at the cell level and thus depends on the photosensitizer and tissue types, the quantum yield η gives the number of singlet oxygen molecules produced per an absorbed photon, which is a constant under ample oxygen supply. However, when insufficient oxygen supply exists, η is also a function of the oxygen concentration, or pO_2, in tissue. The relationship between η and oxygen

concentration can be derived from differential equations modeling the reaction rates of oxygen and photosensitizer in their various states [35,36,39]. Based on our current understanding, the PDT effect is directly proportional to the total concentration of reactions of singlet oxygen $[^1O_2]_{rx}$, with biological targets which can be either calculated (Eq. (3)) or indirectly measured in tissue via the local $^1O_2$ concentration [30,31].

Methods of dosimetry which attempt to measure the various factors which contribute to PDT dose are referred to as 'explicit dosimetry' [34]. In contrast, implicit dosimetry mechanisms rely on the measurement of a surrogate marker for PDT damage, such as photosensitizer photobleaching.

In vivo light dosimetry in PDT

The simplest explicit dosimetry scheme must take into account the fluence of light delivered to the tissue. This is complicated by the fact that the total fluence in tissues is a function not only of the incident light delivered by the laser but also of scattered light. Often clinical PDT treatments are prescribed in terms of the incident light delivered from the laser rather than the total fluence of light the tissues receive, which is a combination of scattered and incident light. Substantial differences in total fluence to tissues can be observed among patients if the clinician accounts only for incident light [40,41]. Dosimetry systems using isotropic light detectors have been developed to measure both incident and scattered light [42,43], including multi-channel systems capable of recording light fluence rate in real-time at multiple sites. These systems should begin to allow clinical researchers to measure and therefore prescribe a consistent total fluence to the tissues. Isotropic detectors are often used to measure the light fluence rate directly [44]. These detectors have the advantage of detecting light from all directions, unlike flat photo-diodes, which can only detect normally incident light [45].

Photosensitizers

Various photosensitizing drugs have been developed. Although Type I photosensitizers have been investigated for antimicrobial applications [46], most available oncologic photosensitizers achieve their cytotoxic effect primarily via Type II reactions. The first-generation photosensitizer, haematoporphyrin derivative (HPD), is a mixture of porphyrin monomers and oligomers that is partially purified to produce the commercially available product porfimer sodium, marketed under the tradename Photofrin®. Photofrin was approved for treatment of early stage lung cancer in 1998, and for Barret's esophagus with high grade dysplasia in 2003. In Canada, Photofrin is also approved for partial or totally obstructing esophageal cancer and transitional cell bladder cancer.

Second generation of photosensitizers try to increase the light penetration depth with longer-wavelength absorption peaks and to reduce the skin photosensitivity by allowing more rapid clearance from skin. Among these are mTHPC (Foscan®), which has been investigated in clinical trials for a variety of tumors and has been approved for palliative treatment in Europe, and Pd-Bacteriopheophorbide (Tookad®) and Motexafin Lutetium® (MLu), which are both currently undergoing Phase I trials for prostate cancer treatment [6–10]. Other second-generation photosensitizers include benzoporphyrin derivative monoacid A (BPD-

MA), or verteporfin. In preclinical trials, it was observed that verteporfin preferentially targeted neovasculature [47,48]. Although not yet applied in human clinical trial, BPD-MA has been tested in animal models for prostate cancer. As understanding of the mechanisms of photosensitizer uptake and preferential sensitization of tumors increases, drugs designed to increase tumor-specific selectivity and light penetration while minimizing sensitization of normal tissue will continue to be developed.

Another development of note is the prodrug δ-aminolevulinic acid (ALA). Unlike other PDT drugs, ALA itself is not a photosensitizer. When taken up by cells, however, it is converted by a naturally occurring biosynthetic process into the photosensitizer protoporphyrin IX (PpIX). ALA can be applied topically, and was approved by the FDA in 1999 for the treatment of actinic keratosis (AK). ALA has the advantage that it clears from normal tissue within days and can be applied topically, so it causes almost no systemic photosensitivity. In order to improve the uptake of ALA, two variants (methyl-and hexyl-aminolevulinate) have been developed. Methylaminolevulinate (*m*-ALA) has been approved for treatment of AK under the name Metvix®. The hexyl variant (*h*-ALA), marketed as Hexvix®, has been approved in the European Union for use in fluorescence cystoscopy. In this case, the preferential accumulation of PpIX in tumors relative to normal bladder endothelium allows tumors to be differentiated by their increased PpIX fluorescence.

Table 1 listed photosensitizers that are or can be used for prostate photodynamic therapy along with essential parameters for photodynamic therapy, such as wavelength of treatment, drug-treatment interval, US or Europe FDA approval dates.

Prostate PDT procedures and clinic trials

Several clinical trials of PDT on prostate have been published in the literature. A trial of interstitial prostate PDT in humans has been reported by Nathan et al. [5], in which 14 men with locally recurrent prostate cancer were treated using meso-tetrahydroxyphenyl chlorin (mTHPC)-mediated interstitial PDT. The light treatment was directed against regions from which biopsies showed cancer or which were suspicious on imaging studies. The entire prostate gland was not treated. The treatment was well tolerated except for incontinence (2 patients) and impotence (2 patients). Post-treatment PSA levels decreased in 9 of 14 patients. There was biopsy and radiographic evidence of response in several patients. The authors concluded that PDT should be further studied in organ-confined prostate cancer.

A clinical trial of ALA-mediated PDT was performed on 14 patients with histologically proven prostate cancer [6]. Patients received ALA of 20 mg/kg body weight orally and were treated with 633nm light through a 1-cm cylindrical diffuser for a total light energy of 250 J/cm. A significant reduction of PSA levels was observed 6 weeks after interstitial PDT.

Phase I & II clinical trials of Tookad®-mediated PDT of patients with locally recurrent prostate cancer after radiotherapy are ongoing at the University of Toronto [7–10]. The treatment is performed using interstitial linear sources with Tookad drug dose of 2 mg/kg and 763nm light energy of 100–360 J/cm of linear source starting at 6–10 min after drug injection for a light treatment time of 17–30 min [10]. This is a vascular targeted PDT since the drug perfusion is very fast. Since the light penetration at 763nm is up to 3 cm, six equal

spaced linear sources are sufficient to cover the entire gland. Current protocol does not require *in vivo* light dosimetry.

A Phase I clinical trial of motexafin lutetium (MLu)-mediated PDT in patients with locally recurrent prostate carcinoma was initiated at the University of Pennsylvania [7,8]. The protocol was approved by the Institutional Review board of the University of Pennsylvania, the Clinical Trials and Scientific Monitoring Committee (CTSRMC) of the University of Pennsylvania Cancer Center, and the Cancer Therapy Evaluation Program (CTEP) of the National Cancer Institute. A total of 18 patients were treated, of which 17 patients have undergone measurement of optical properties (one patient yielded no results due to heavy bleeding). Each patient gave informed consent and underwent an evaluation, which included an MRI of the prostate, bone scan, laboratory studies including PSA, and a urological evaluation. Approximately 2 weeks prior to the scheduled treatment a transrectal ultrasound (TRUS) was performed for treatment planning. An urologist drew the target volume (the prostate) on each slice of the ultrasound images. These images were spaced 0.5 cm apart and were scanned with the same ultrasound unit used for treatment.

All light sources and detectors were inserted into the prostate via transparent plastic catheters (Flexi-needle, Best Medical International, Spring-field, VA). The catheters were aligned to the prostate using a template attached to the TRUS unit, as shown in Fig. 2(A). The template provided a grid of possible catheter positions separated by 0.5 cm in the lateral and vertical directions. The TRUS unit is calibrated to superimpose these positions on the ultrasound images it acquires, as shown in Fig. 2(B). A treatment plan was then prepared to determine the locations and lengths of the light sources. Cylindrical diffusing fibers (CDF) with active lengths 1–5 cm were used as light sources. The CDF sources were parallel, spaced 1 cm apart and the light power per unit length was less than or equal to 150mW/cm for each CDF. The length of the CDF (shaded region in Fig. 2(A)) at a particular position within the prostate was selected to cover the full length of the prostate. For practical reasons, clinical application often required that the prostate be divided into four quadrants. Four isotropic detectors were used, each placed in the center of one quadrant. A fifth isotropic detector was placed in a urethral catheter to monitor the light fluence in the urethra (Fig. 2(B)).

The patients were anesthetized in the operating room with general anesthesia to minimize patient movement during the procedure. Transrectal ultrasound-guided biopsies for MLu measurements were obtained prior to light delivery. The ultrasound unit was used to guide needle placement in the operating room. Four detector catheters (one for each quadrant) were inserted into the prostate, as indicated by the ‘x’ symbols in Fig. 2(B). These detectors were kept in place during the entire procedure of PDT treatment. Four additional pre-planned treatment catheters for light sources (filled circles) were then inserted 0.5 or 0.7 cm away from the detector catheters. These source catheters were used for both light delivery and measurement of optical properties. A 15-W diode laser, model 730 (Diomed Ltd., Cambridge, United Kingdom) was used as the 732nm light source.

Current state of art prostate PDT protocols base the prescription of light fluence on direct *in vivo* measurements with isotropic detectors. To determine the three-dimensional coverage,

the light fluence can be calculated using the diffusion model directly (Eq. (4)) or the analytical model for point sources (Eq. (5)), which can be used to make up linear light source geometry, if the optical properties can be determined for the prostate right before PDT [49,50].

In our current clinical protocol, we expect to complete at least 11 dosimetry schemes. Each corresponds to the MLu drug level (in mg/kg), the drug-light interval (in hours), and the total light fluence (in J/cm^2). The maximally tolerated dose (MTD) is defined as the highest PDT dose which results in less than two instances of dose-limiting toxicity (DLT) among 12 treated patients [7]. DLT is defined as Grade III non-hematologic or Grade IV hematologic toxicity. Currently we have fixed the MLu drug level at 2 mg/kg and drug-light interval at 3 h. The current light fluence is at 150 J/cm^2.

Interstitial PDT dosimetry

In vivo characterization of tissue optical properties

The measurement of light fluence rate *in vivo* is necessary but not sufficient to quantify light fluence rate distribution. Volumetric determination of the light fluence rate in the entire treatment volume requires accurate characterization of the *in vivo* tissue optical properties as input (μ_a, μ_s' in Eq. (4)). Several techniques have been developed to determine the optical properties *in vivo* [24,51].

The most widely used model of light transport in tissue is the radiative transport equation [52]. Because analytic solutions to this equation exist for only very simple geometries, it is generally solved by a Taylor expansion. A first-order expansion yields the commonly used diffusion approximation. In the near infrared (NIR) region, tissue scattering dominates over tissue absorption, so that the diffusion approximation is valid [53]. Under diffusion approximation, the light fluence rate, φ, can be described by

$$\frac{\partial\phi(r,t)}{\partial t}=\nabla(Dv)\nabla\phi(r,t)-v\mu_a\phi(r,t)+S(r,t), \quad (4)$$

where v is the speed of light in the turbid medium; $D=1/3\mu_s'$ is the photon diffusion coefficient; S is an isotropic source term which gives the number of photons emitted at position r and time t per unit volume per unit time.

With the diffusion approximation, the light fluence rate φ at a distance r from a point source can be expressed as [54]

$$\phi=\frac{S\times\mu_{eff}^2}{4\pi r\times\mu_a}\times e^{-\mu_{eff}\times r}=\frac{S\times 3\mu_s'}{4\pi r}\times e^{-\mu_{eff}\times r} \quad (5)$$

where S is the power of the point source (mW); $\varphi(r)$ is the the fluence rate (mW/cm^2); the quantity $\mu_{eff}=\sqrt{3\times\mu_a\times\mu_s'}$ is the effective attenuation coefficient in tissues, applicable

over a wider range of μ_a and μ_s' than the traditional definition $\mu_{eff} = \sqrt{3 \times \mu_a \times (\mu_s' + \mu_a)}$ [55].

In theory, measurements of φ at two different distances r from a point source of known power S are sufficient to determine both μ_a and μ_s'. The two free parameters (μ_a and μ_s') are inherently separable because for a CDF of given length the magnitude of the fluence rate near the light source (h=0) is determined by μ_s' only and the slope of the spatial decay of the light fluence rate is determined by μ_{eff} only. Measurements at multiple sites allow evaluating the variation of these optical characteristics within the prostate volume. Since Eq. (5) is a non-linear equation of two free parameters μ_a and μ_s', we used a differential evolution algorithm developed by Storn and Price [56]. This algorithm is simple and robust, and converges faster and with more certainty than both the adaptive simulated annealing and the annealed Nelder & Mead approach. We modified the algorithm to require that all parameters (μ_a and μ_s') were positive [57].

To implement this model in our clinical protocol, we have developed a computer-controlled positioning system capable of moving an isotropic point source and an isotropic detector independently along parallel catheters in the prostate [22]. As a result, fluence rates can be measured at a variety of distances from the point source, and the resulting profile can be used to determine the prostate optical properties. By moving the source to various positions, we can map the distribution of optical properties throughout the organ [58]. Fig. 3 shows measured distribution of optical properties in human prostate. Clearly, there is a significant difference (up to three times) between optical properties measured in different locations, which will affect the light fluence distribution.

Within a prostate gland, the optical properties can be measured at various sites. Fig. 4 shows the measured optical properties (μ_a and μ_{eff}) in several human prostate glands before and after PDT. The effective absorption coefficients change by three times over the length of prostate, indicating significant changes of light penetration depth at different locations within a prostate. [22] If one performs a sufficient number of measurements in three dimensions, it is possible to reconstruct a 3D map of optical properties. Preliminary results are shown in Fig. 5 for the *in vivo* absorption and reduced scattering coefficients at the treatment wavelength (732 nm) in a human prostate. In each figure, the color indicates the absorption or scattering coefficient of the prostate at a given position in one transverse slice. The prostate (blue), urethra (red) and rectal wall (green) were identified on the corresponding ultrasound image (not shown). To generate these images, measurements taken at point-by-point at the center of 6 source positions and 12 detector positions per slice and fitted using the non-linear fitting model described previously. The current methods limited this to 0.5×0.5 cm^2 resolution. Further improvements are possible by solving the diffusion equation directly using finite-element methods.

Quantification of drug concentration and tissue oxygenation

Determination of drug concentration is important for PDT efficacy. Early PDT clinical protocols only specify this quantity in terms of the amount of photosensitizer given to

patient per body weight. Recent *in vivo* studies have shown large variation of photosensitizer concentration in different tissue types, thus suggesting determination of this quantity *in vivo* in the region of treatment directly [22,58]. To include the drug concentration in the evaluation of PDT dose, *in situ* fluorescence [59] or absorption [39,60–63] measurements of photosensitizer can be made interstitially using optical fibers. Absorption spectroscopy has the advantage that, in addition to drug concentration, tissue hemodynamics can be monitored, which is important because tissue oxygenation is known to affect PDT efficacy *in vitro* [36,64]. Changes in tissue oxygenation due to photochemical oxygen consumption during PDT have been observed directly [65,66], and indirectly through their effect on the photobleaching rate [39,67–70]. Recent studies have shown that the concentrations of hemoglobin (Hb), HbO_2, H_2O, and photosentizers can be determined from absorption measurements [24,60–63,71]. In our current prostate protocol, we accomplish this by repeating the absorption measurements described above, but replacing the laser source with a white light source and the photodiode with a spectrograph. The result is a fluence rate profile as a function of source-detector distance for each wavelength from 600 to 850 nm. These data can be fit using techniques similar to those described above to obtain scattering and absorption spectra of the tissue being interrogated. The resulting absorption spectrum is then fit using the singular value decomposition algorithm to obtain the contributions of oxy- and deoxyhemoglobin and photosensitizer. Fig. 6(a) shows measured distribution of Hb and $StO_2 = HbO_2/Hb$ measured in human prostate [58].

The drug concentration can also be determined using fluorescence spectroscopy. To accomplish this in our prostate PDT protocol, we have designed a side-firing optical probe which can be inserted into the same catheters used for absorption measurements [26]. The same probe is used to deliver excitation light and collect fluorescence. The collected fluorescence is separated from reflected excitation light by a dichroic beamsplitter. The probe is positioned by the motorized positioners, and acquires fluorescence spectra every 2mm along the catheter. The fluorescence measured by this probe is corrected for optical properties using an analytical correction algorithm and fit to determine the contributions of MLu and background fluorescence [26]. Fig. 6(b) shows measured distribution of MLu drug concentration in prostate determined by absorption measurements at 732 nm, absorption spectroscopy measurements (see below) and fluorescence measurements [58]. The results of the three methods agree well for MLu drug concentration.

Optimization of prostate PDT delivery

We have developed a Cimmino algorithm to optimize the PDT dose distribution in prostate by adjusting the location, length, and intensity of light source strengths [72]. The Cimmino algorithm is an iterative linear algorithm that solves linear equations. The algorithm is safer than most common optimization algorithms since it always converges and, if all the constraints are not all satisfied, it reverts to the least-square solution. Notice that the relationship between the light fluence rate and the power of point (or linear) source is linear even though the relationship between the light fluence rate and the distances from the light source is non-linear. Preliminary results indicate that it is possible to cover the prostate gland while reduce the PDT dose to critical organs in homogeneous prostate. The algorithm

is fast enough to perform the task in near-real-time (e.g., 300 s) on a PC. Further studies are undergoing to optimize PDT dose in heterogeneous medium.

Implicit real-time PDT dosimetry and feedback light delivery

Implicit dosimetry monitors a dosimetry quantity such as fluorescence photobleaching or blood flow in real-time. Such a quantity may correlate with the PDT efficacy directly. Preclinical studies in mice have shown clear correlation between blood flow [73] and blood oxygenation [74] and tumor regrowth rate. Real-time monitoring of both quantities is ongoing for human prostate [75], which may lead to a simple dosimetric quantity which correlates directly with the PDT outcome.

With real-time PDT dosimetry, it is possible to use the measured quantities as a feedback to adjust the light source strengths in real-time to optimize PDT dose and/or implicit dosimetric quantities.

Conclusions

We would advocate a comprehensive approach for interstitial PDT dosimetry for all future clinical PDT protocols. At the minimum, this should involve quantitative measurement of the essential explicit dosimetric parameters such as light fluence rate, tissue optical properties, and photosensitizer concentration. Given an appropriate model, the local tissue oxygenation should also be taken into account. In addition, implicit dosimetric indicators of PDT effect, such as fluorescence photobleaching or blood flow, may prove valuable.

Acknowledgments

This work is supported by Department of Defense (DOD), US Medical Research and Material Command, grant DAMD17-03-1-0132 and National Institutes of Health (NIH), R01 CA109456-01A1 and P01 CA87971-01A1.

Abbreviations

ALA	5-aminolevulinic Acid
BPD-MA	benzoporphyrin derivative monoacid A
CW	continuous wave
FDA	Food and Drug Administration
Hb	hemoglobin
HPD	hematoporphyrin derivative
ISC	intersystem crossing
LS-11	taloporfin sodium
MLu	motexafin lutetium
mTHPC	meso-tetrahydroyphenol chlorin
PC4	silicon pthalocyanine 4

PDT	photodynamic therapy
PpIX	protoporphyrin IX
Tookad	Pd-Bacteriopheophorbide

References

1. Jemal A, Seigel R, Ward E, et al. Cancer Statistics, 2006. CA-A Cancer J Clin. 2006; 56:106–30.
2. Catalona WJ. Screening for early detection. Lancet. 1996; 347:883–4. [PubMed: 8622399]
3. Dougherty TJ, Gomer DJ, Henderson BW, et al. Photodynamic Therapy. J Natl Cancer Inst. 1998; 90:889–905. [PubMed: 9637138]
4. Ornstein DKO, Herschman JD, Andriole GL. Evaluation and management of the man who has failed primary curative therapy for prostate cancer. Urol Clin North Am. 1998; 25:591–601. [PubMed: 10026768]
5. Nathan TR, Whitelaw DE, Chang SC, et al. Photodynamic therapy for prostate cancer recurrence after radiotherapy: a Phase I study. J Urol. 2002; 168:1427–32. [PubMed: 12352410]
6. Zaak D, Sroka R, Hoppner M, et al. Photodynamic therapy by means of 5-ALA induced PPIX in human prostate—preliminary results. Med Laser Appl. 2003; 18:91–5.
7. Stripp DCH, Mick R, Zhu TC, et al. Phase I trial of Motexafin lutetium-mediated interstitial photodynamic therapy in patients with locally recurrent prostate cancer. Proc SPIE. 2004; 5315:88–99.
8. Verigos K, Stripp DCH, Mick R, et al. Updated results of a phase I trial of motexafin lutetium-mediated interstitial photodynamic therapy in patients with locally recurrent prostate cancer. J Environ Pathol Toxicol Oncol. 2006; 25(1–2):373–88. [PubMed: 16566729]
9. Weersink RA, Bogaards A, Gertner M, et al. Techniques for delivery and monitoring of TOOKAD (WST09)-mediated photodynamic therapy of the prostate: clinical experience and practicalities. J Photochem Photobiol B. 2005; 79(3):211–22. [PubMed: 15896648]
10. Weersink RA, Forbes J, Bisland S, et al. Assessment of cutaneous photosensitivity of TOOKAD (WST09) in preclinical animal models and in patients. Photochem Photobiol. 2005; 81(1):106–13. [PubMed: 15382963]
11. Pinthus JH, Bogaards A, Weersink R, Wilson BC, Tracht-enberg J. Photodynamic therapy for urological malignancies: past to current approaches. J Urol. 2006; 175(4):1201–7. [PubMed: 16515960]
12. Arnfield MR, Chapman JD, Tulip J, Fenning MC, McPhee MS. Optical properties of experimental prostate tumors in vivo. Photochem Photobiol. 1993; 57(2):306–11. [PubMed: 8451295]
13. Chen Q, Wilson BC, Shetty SD, Patterson MS, Cerny JC, Hetzel FW. Changes in in vivo optical properties and light distributions in normal canine prostate during photodynamic therapy. Radiat Res. 1997; 147(1):86–91. [PubMed: 8989374]
14. Lee LK, Whitehurst C, Chen Q, Pantelides ML, Hetzel FW, Moore JV. Interstitial photodynamic therapy in the canine prostate. Br J Urol. 1997; 80(6):898–902. [PubMed: 9439405]
15. Selman SH, Keck RW. The effect of tranurethral light on the canine prostate after sensitization with the photosensitizer tin (II) etiopurpurin dichloride: a pilot study. J Urol. 1994; 152:2129–32. [PubMed: 7966701]
16. Selman SH, Keck RW, Hampton JA. Transperineal photodynamic ablation of the canine prostate. J Urol. 1996; 156:258–60. [PubMed: 8648818]
17. Selman SH, Albrecht D, Keck RW, Brennan P, Kondo S. Studies of tin ethyl etiopurpurin photodynamic therapy of the canine prostate. J Urol. 2001; 165:1795–801. [PubMed: 11342978]
18. Hsi A, Kapatkin AS, Strandberg J, et al. Photodynamic therapy in the canine prostate using Motexafin lutetium. Clin Cancer Res. 2001; 7:651–60. [PubMed: 11297261]

19. Chang SC, Buonaccorsi G, MacRobert A, Brown SG. Interstitial photodynamic therapy in the canine prostate with disulfonated aluminum phthalocyanine and 5-aminolevulinic acid-induced photoporphyrin IX. Prostate. 1997; 32:89–98. [PubMed: 9215396]
20. Chang SC, Buonaccorsi G, MacRobert A, Bown SG. Interstitial and transurethral photodynamic therapy of the canine prostate using *meso*-tetra-(*m*-hydroxyphenyl) chlorin. Int J Cancer. 1996; 67:555–62. [PubMed: 8759616]
21. Dimofte A, Finlay JC, Zhu TC. A method for determination of the absorption and scattering properties interstitially in turbid media. Phys Med Biol. 2005; 50:2291–311. [PubMed: 15876668]
22. Zhu TC, Dimofte A, Finlay JC, et al. Optical properties of human prostate at 732 nm measured in vivo during Motexafin lutetium-mediated photodynamic therapy. Photochem Photobiol. 2005; 81:96–105. [PubMed: 15535736]
23. Finlay JC, Zhu TC, Dimofte A, et al. In vivo determination of the absorption and scattering spectra of the human prostate during photodynamic therapy. Proc SPIE. 2004; 5315:132–42.
24. Wang HW, Zhu TC, Putt ME, et al. In-vivo broadband reflectance measurements of light penetration depth, blood oxygenation, hemoglobin concentration, and drug concentration in human tissues before and after photodynamic therapy. J Biomed Opt. 2005; 10(1–13)
25. Finlay JC, Zhu TC, Dimofte A, et al. In vivo measurement of fluorescence emission in the human prostate during photodynamic therapy. Proc SPIE. 2005; 5689:299–310.
26. Finlay JC, Zhu TC, Dimofte A, Stripp D, Malkowicz SB, Busch TM, Hahn SM. Interstitial fluorescence spectroscopy in the human prostate during motexafin lutetium-mediated photodynamic therapy. Photochem Photobiol. 2006 submitted for publication.
27. Pass HI. Photodynamic therapy in oncology: mechanisms and clinical use. J Natl Cancer Inst. 1993; 85(6):443–56. [PubMed: 8445672]
28. Ochsner M. Photophysical and photobiological processes in the photodynamic therapy of tumours. J Photochem Photobiol B. 1997; 39(1):1–18. [PubMed: 9210318]
29. Foote CS. Photosenstizied oxidations and the role of singlet oxygen. Acc Chem Res. 1967; 1:104–10.
30. Niedre M, Patterson MS, Wilson BC. Direct near-infrared luminescence detection of singlet oxygen generated by photodynamic therapy in cells in vitro and tissues in vivo. Photochem Photobiol. 2002; 75(4):382–91. [PubMed: 12003128]
31. Niedre MJ, Patterson MS, Giles A, Wilson BC. Imaging of photodynamically generated singlet oxygen luminescence in vivo. Photochem Photobiol. 2005; 81(4):941–3. [PubMed: 15865471]
32. Mang TS, Dougherty TJ, Potter WR, Boyle DG, Somer S, Moan J. Photobleaching of porphyrins used in photodynamic therapy and implications for therapy. Photochem Photobiol. 1987; 45:501–6. [PubMed: 3575444]
33. Jacques SL, Joseph R, Gofstein G. How photobleaching effects dosimetery and fluorescence monitoring of PDT in turbid media. Proc SPIE. 1993; 1881:168–79.
34. Wilson BC, Patterson MS, Lilge L. Implicit and explicit dosimetry in photodynamic therapy: a new paradigm. Lasers Med Sci. 1997; 12:182–99. [PubMed: 20803326]
35. Georgekoudi I, Foster TH. Singlet oxygen-versus nonsinglet oxygen-mediated mechanisms of sensitizer photo-bleaching and their effects on photodynamic dosimetry. Photochem Photobiol. 1998; 67:612–25. [PubMed: 9648527]
36. Georgakoudi I, Nichols MG, Foster TH. The mechanism of Photofrin photobleaching and its consequences for photodynamic dosimetry. Photochem Photobiol. 1997; 65:135–44. [PubMed: 9066293]
37. Patterson MS, Wilson BC, Graff R. In vivo tests of the concept of photodynamic threshold dose in normal rat liver photosensitized by aluminum chlorosulphonated phthalocyanine. Photochem Photobiol. 1990; 51:343–9. [PubMed: 2356229]
38. Hetzel, FW.; Brahmavar, SM.; Chen, Q.; Jacques, SL.; Patterson, MS.; Wilson, BC.; Zhu, TC. Photodynamic Therapy Dosimetry, AAPM Report No. 88. Madison, WI: Med Phys Publishing; 2005.
39. Finlay JC, Mitra S, Foster TH. Photobleaching kinetics of Photofrin in vivo and in multicell tumor spheroids indicate multiple simultaneous bleaching mechanisms. Phys Med Biol. 2004; 49:4837–60. [PubMed: 15584523]

40. Star WM. Light dosimetry in vivo. Phys Med Biol. 1997; 42:763–87. [PubMed: 9172258]
41. Dimofte A, Zhu TC, Hahn SM, Lustig RA. In vivo light dosimetry for motexafin lutetium-mediated PDT of recurrent breast cancer. Lasers Surg Med. 2002; 31(5):305–12. [PubMed: 12430147]
42. Baas P, Murrer L, Zoetmulder FA, Stewart FA, Ris HB, van Zandwijk N, Peterse JL, Rutgers EJ. Photodynamic therapy as adjuvant therapy in surgically treated pleural malignancies. Br J Cancer. 1997; 76(6):819–26. [PubMed: 9310252]
43. Solonenko M, Zhu TC, Vulcan TG. Commissioning of the isotropic light dosimetry system for photodynamic therapy. Med Phys. 1999; 26:1124.
44. van Staveren HJ, Marijnissen HPA, Aalders MC, Star WM. Construction, quality assurance, and calibration of spherical isotropic fibre optic light diffusers. Lasers Med Sci. 1995; 10:137–47.
45. Vulcan TG, Zhu TC, Rodriguez CE, et al. Comparison between isotropic and nonisotropic dosimetry systems during intraperitoneal photodynamic therapy. Lasers Surg Med. 2000; 26(3): 292–301. [PubMed: 10738292]
46. Wainwright M. Photodynamic antimicrobial chemotherapy (PACT). J Antimicrob Chemother. 1998; 42(1):13–28. [PubMed: 9700525]
47. Momma T, Hamblin MR, Wu HC, Hasan T. Photodynamic therapy of orthotopic prostate cancer with benzoporphyrin derivative: local control and distant metastasis. C ancer Res. 1998; 58(23): 5425–31.
48. Chen B, Pogue BW, Zhou X, et al. Effect of of tumor host microenvironment on photodynamic therapy in a rat prostate tumor model. Clin Cancer Res. 2005; 11(2 Part 1):720–7. [PubMed: 15701861]
49. Zhu TC, Li J, Finlay JC, et al. In-vivo light dosimetry of interstitial PDT of human prostate. Proc SPIE. 2006; 6139(61390):L1–11.
50. Li J, Zhu TC, Finlay JC. Study of light fluence rate distribution in photodyanmic therapy using finite-element method. Proc SPIE. 2006; 6139(61390):M1–8.
51. Zhu TC, Hahn SM, Kapatkin AS, et al. In-vivo optical properties of normal canine prostate at 732 nm using motexafin lutetium-mediated photodynamic therapy. Photochem Photobiol. 2003; 77:81–8. [PubMed: 12856887]
52. Ishimaru, A. Wave propagation and scattering in random media. New York: IEEE Press; 1997.
53. Wilson, BC.; Patterson, MS. The determination of light fluence distribution in photodynamic therapy. In: Kessel, D., editor. Photodynamic therapy of neoplastic disease. Boca Raton: CRC Press Inc; 1990. p. 129-44.
54. Jacques S. Light distributions from point, line and plane sources for photochemical reactions and fluorescence in turbid biological tissues. Photochem Photobiol. 1998; 67:23–32. [PubMed: 9477762]
55. Nakai T, Nishimura G, Yamamoto K, Tamura M. Expression of optical diffusion coefficient in high-absorption turbid media. Phys Med Biol. 1997; 42:2541–9. [PubMed: 9434306]
56. Storn R, Price K. Differential evolution - a simple and efficient heuristic for global optimization over continuous spaces. J Global Optimization. 1997; 11:341–59.
57. Zhu TC, Bjarngard BE, Xiao Y, Yang CJ. Modeling the output ratio in air for megavoltage photon beams. Med Phys. 2001; 28(6):925–37. [PubMed: 11439489]
58. Zhu TC, Finlay JC, Hahn SM. Determination of the distribution of light, optical properties, drug concentration, and tissue oxygenation in-vivo in human prostate during Motexafin lutetium-mediated photodynamic therapy. J Photochem Photobiol B. 2005; 79:231–41. [PubMed: 15896650]
59. Diamond KR, Patterson MS, Farrell TJ. Quantification of fluorophore concentration in tissue-simulating media by fluorescence measurements with a single optical fiber. Appl Opt. 2003; 42:2436–42. [PubMed: 12737480]
60. Liu H, Boas DA, Zhang Y, Yodh AG, Chance B. Determination of optical properties and blood oxygenation in tissue using continuous near-infrared light. Phys Med Biol. 1995; 40:1983–93. [PubMed: 8587945]

61. Kienle A, Lilge L, Patterson MS, Hibst R, Steiner RA, Wilson BC. Spatially resolved absolute diffuse reflectance measurements for noninvasive determination of the optical scattering and absorptions of biological tissue. Appl Opt. 1996; 35:2304–13. [PubMed: 21085367]
62. Doornbos RMP, Lang R, Aalders MC, Cross FW, Sterenborg HJ. The determination of in vivo human tissue optical properties and absolute chromophore concentrations using spatially resolved steady-state diffuse reflectance spectroscopy. Phys Med Biol. 1999; 44:967–81. [PubMed: 10232809]
63. Solonenko M, Cheung R, Busch TM, et al. In-vivo reflectance measurement of motexafin lutetium uptake, optical properties, and oxygenation of canine large bowels, kidneys, and prostates. Phys Med Biol. 2002; 47:857–73. [PubMed: 11936174]
64. Nichols MG, Foster TH. Oxygen diffusion and reaction kinetics in the photodynamic therapy of multicell tumour spheroids. Phys Med Biol. 1994; 39:2161–81. [PubMed: 15551546]
65. Tromberg BJ, Orenstein A, Kimel S, et al. In vivo tumor oxygen tension measurements for the evaluation of the efficiency of photodynamic therapy. Photochem Photobiol. 1990; 52:375–85. [PubMed: 2145595]
66. Henderson BW, Busch TM, Vaughan LA, et al. Photofrin photodynamic therapy can significantly deplete or preserve oxygenation in human basal cell carcinomas during treatment, depending on fluence rate. Cancer Res. 2000; 60:525–9. [PubMed: 10676629]
67. Robinson DJ, de Bruijn HS, van der Veen N, Stringer MR, Brown SB, Star WM. Fluorescence photobleaching of ALA-induced protoporphyrin IX during photodynamic therapy of normal hairless mouse skin: the effect of light dose and irradiance and the resulting biological effect. Photochem Photobiol. 1998; 67:140–9. [PubMed: 9477772]
68. Robinson DJ, de Bruijn HS, van der Veen N, Stringer MR, Brown SB, Star WM. Protoporphyrin IX fluorescence photobleaching during ALA-mediated photodynamic therapy of UVB-induced tumors in hairless mouse skin. Photochem Photobiol. 1999; 69:61–70. [PubMed: 10063801]
69. Finlay JC, Conover DL, Hull EL, Foster TH. Porphyrin bleaching and PDT-induced spectral changes are irradiance dependent in ALA-sensitized normal rat skin in vivo. Photochem Photobiol. 2001; 73:54–63. [PubMed: 11202366]
70. Finlay JC, Mitra S, Foster TH. In vivo mTHPC photobleaching in normal rat skin exhibits unique irradiance-dependent features. Photochem Photobiol. 2002; 75:282–8. [PubMed: 11950094]
71. Finlay JC, Foster TH. Hemoglobin oxygen saturations in phantoms and in vivo from measurements of steady state diffuse reflectance at a single, short source-detector separation. Med Phys. 2004; 31(7):1949–59. [PubMed: 15305445]
72. Altschuler MD, Zhu TC, Li J, Hahn SM. Optimized interstitial PDT prostate treatment planning with the Cimmino feasibility algorithm. Med Phys. 2005; 32(12):3524–36. [PubMed: 16475751]
73. Yu G, Durduran T, Zhou C, et al. Noninvasive monitoring of murine tumor blood flow during and after photodynamic therapy provides early assessment of therapeutic efficacy. Clin Cancer Res. 2005; 11(9):3543–52. [PubMed: 15867258]
74. Wang HW, Putt ME, Emanuele MJ, et al. Treatment-induced changes in tumor oxygenation predict photodynamic therapy outcome. Cancer Res. 2004; 64(20):7553–61. [PubMed: 15492282]
75. Yu G, Durduran T, Zhou C, Zhu TC, Finlay JC, Busch TM, Malkowicz SB, Hahn SM, Yodh AG. Real-time in situ monitoring of human prostate photodynamic therapy with diffuse light. Photochem Photobiol. 2006 Epub ahead of print.
76. Chen Q, Hetzel FW. Laser dosimetry studies in the prostate. J Clin Laser Med Surg. 1998; 16(1): 9–12. [PubMed: 9728124]
77. Chapman JD, McPhee MS, Walz N, et al. Nuclear magnetic resonance spectroscopy and sensitizer-adduct measurements of photodynamic therapy-induced ischemia in solid tumors. J Natl Cancer Inst. 1991; 83(22):1650–9. [PubMed: 1749018]
78. Lapointe D, Brasseur N, Cadorette J, et al. High-resolution PET imaging for in vivo monitoring of tumor response after photodynamic therapy in mice. J Nucl Med. 1999; 40(5):876–82. [PubMed: 10319764]
79. Igbaseimokumo U. Quantification of in vivo Photofrin uptake by human pituitary adenoma tissue. J Neurosurg. 2004; 101(2):272–7. [PubMed: 15309918]

80. Marks PV, Belchetz PE, Saxena A, et al. Effect of photo-dynamic therapy on recurrent pituitary adenomas: clinical phase I/II trial—an early report. Br J Neurosurg. 2000; 14(4):317–25. [PubMed: 11045196]
81. Wiedmann M, Berr F, Schiefke I, et al. Photodynamic therapy in patients with non-resectable hilar cholangiocarcinoma: 5-year follow-up of a prospective phase II study. Gastrointest Endosc. 2004; 60(1):68–75. [PubMed: 15229428]
82. Wiedmann M, Caca K, Berr F, et al. Neoadjuvant photodynamic therapy as a new approach to treating hilar cholangiocarcinoma: a phase II pilot study. Cancer. 2003; 97(11):2783–90. [PubMed: 12767091]
83. Cuenca RE, Allison RR, Sibata C, Downie GH. Breast cancer with chest wall progression: treatment with photodynamic therapy. Ann Surg Oncol. 2004; 11(3):322–7. [PubMed: 14993029]
84. Touma D, Yaar M, Whitehead S, Konnikov N, Gilchrest BA. A trial of short incubation, broad-area photodynamic therapy for facial actinic keratoses and diffuse photodamage. Arch Dermatol. 2004; 140(1):33–40. [PubMed: 14732657]
85. Ericson MB, Sandberg C, Stenquist B, et al. Photodynamic therapy of actinic keratosis at varying fluence rates: assessment of photobleaching, pain and primary clinical outcome. Br J Dermatol. 2004; 151(6):1204–12. [PubMed: 15606516]
86. Kelty CJ, Ackroyd R, Brown NJ, Brown SB, Reed MW. Comparison of high- vs low-dose 5-aminolevulinic acid for photodynamic therapy of Barrett's esophagus. Surg Endosc. 2004; 18(3): 452–8. [PubMed: 14752635]
87. Hage M, Siersema PD, van Dekken H, et al. 5-Aminolevulinic acid photodynamic therapy versus argon plasma coagulation for ablation of Barrett's oesophagus: a randomised trial. Gut. 2004; 53(6):785–90. [PubMed: 15138203]
88. Hage M, Siersema PD, Vissers KJ, et al. Molecular evaluation of ablative therapy of Barrett's oesophagus. J Pathol. 2005; 205(1):57–64. [PubMed: 15586364]
89. Cappugi P, Mavilia L, Campolmi P, Reali EF, Mori M, Rossi R. New proposal for the treatment of nodular basal cell carcinoma with intralesional 5-aminolevulinic acid. J Chemother. 2004; 16(5): 491–3. [PubMed: 15565918]
90. Loning M, Diddens H, Kupker W, Diedrich K, Huttmann G. Laparoscopic fluorescence detection of ovarian carcinoma metastases using 5-aminolevulinic acid-induced protoporphyrin IX. Cancer. 2004; 100(8):1650–6. [PubMed: 15073853]
91. Frei KA, Bonel HM, Frick H, Walt H, Steiner RA. Photodynamic detection of diseased axillary sentinel lymph node after oral application of aminolevulinic acid in patients with breast cancer. Br J Cancer. 2004; 90(4):805–9. [PubMed: 14970857]
92. Webber J, Fromm D. Photodynamic therapy for carcinoma in situ of the anus. Arch Surg. 2004; 139(3):259–61. [PubMed: 15006881]
93. Dragieva G, Hafner J, Dummer R, et al. Topical photodynamic therapy in the treatment of actinic keratoses and Bowen's disease in transplant recipients. Transplantation. 2004; 77(1):115–21. [PubMed: 14724445]
94. Dragieva G, Prinz BM, Hafner J, et al. A randomized controlled clinical trial of topical photodynamic therapy with methyl aminolaevulinate in the treatment of actinic keratoses in transplant recipients. Br J Dermatol. 2004; 151(1):196–200. [PubMed: 15270891]
95. Rhodes LE, de Rie M, Enstrom Y, et al. Photodynamic therapy using topical methyl aminolevulinate vs surgery for nodular basal cell carcinoma: results of a multicenter randomized prospective trial. Arch Dermatol. 2004; 140(1):17–23. [PubMed: 14732655]
96. Lui H, Hobbs L, Tope WD, et al. Photodynamic therapy of multiple nonmelanoma skin cancers with verteporfin and red light-emitting diodes: two-year results evaluating tumor response and cosmetic outcomes. Arch Dermatol. 2004; 140(1):26–32. [PubMed: 14732656]
97. Azab M, Boyer DS, Bressler NM, et al. Verteporfin therapy of subfoveal minimally classic choroidal neovascularization in age-related macular degeneration: 2-year results of a randomized clinical trial. Arch Ophthalmol. 2005; 123(4):448–57. [PubMed: 15824216]
98. Hopper C, Kubler A, Lewis H, Tan IB, Putnam G. mTHPC-mediated photodynamic therapy for early oral squamous cell carcinoma. Int J Cancer. 2004; 111(1):138–46. [PubMed: 15185355]

99. Lou PJ, Jager HR, Jones L, Theodossy T, Bown SG, Hopper C. Interstitial photodynamic therapy as salvage treatment for recurrent head and neck cancer. Br J Cancer. 2004; 91(3):441–6. [PubMed: 15238981]

100. Shikowitz MJ, Abramson AL, Steinberg BM, et al. Clinical trial of photodynamic therapy with *meso*-tetra (hydroxyphenyl) chlorin for respiratory papillomatosis. Arch Otolaryngol Head Neck Surg. 2005; 131(2):99–105. [PubMed: 15723939]

101. Chou TM, Woodburn KW, Cheong WF, et al. Photodynamic therapy: applications in atherosclerotic vascular disease with motexafin lutetium. Catheter Cardiovasc Interv. 2002; 2002(3):387–94. [PubMed: 12410519]

102. Kereiakes DJ, Szyniszewski AM, Wahr D, et al. Phase I drug and light dose-escalation trial of motexafin lutetium and far red light activation (phototherapy) in subjects with coronary artery disease undergoing percutaneous coronary intervention and stent deployment: procedural and long-term results. Circulation. 2003; 108(11):1310–5. [PubMed: 12939212]

103. Lustig RA, Vogl TJ, Fromm D, et al. A multicenter Phase I safety study of intratumoral photoactivation of talaporfin sodium in patients with refractory solid tumors. Cancer. 2003; 98(8):1767–71. [PubMed: 14534895]

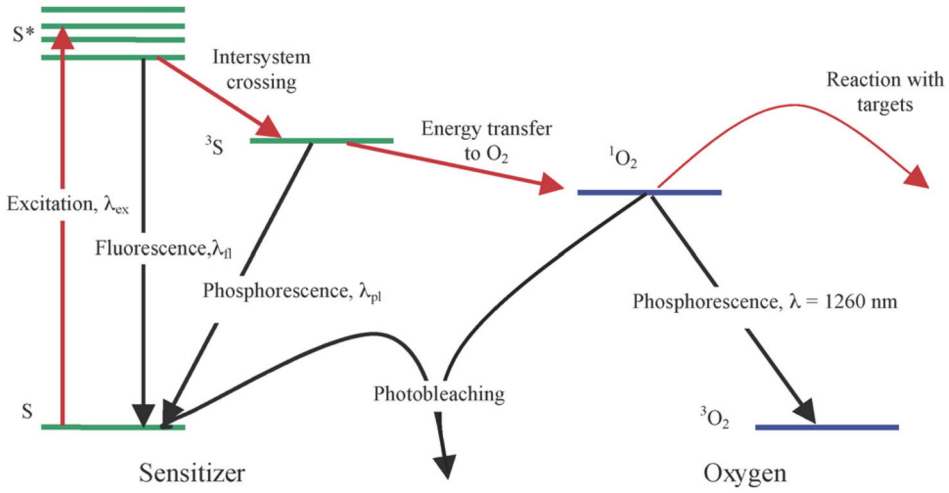

Figure 1.
Energy level diagram illustrating a typical Type II photosensitizer and oxygen.

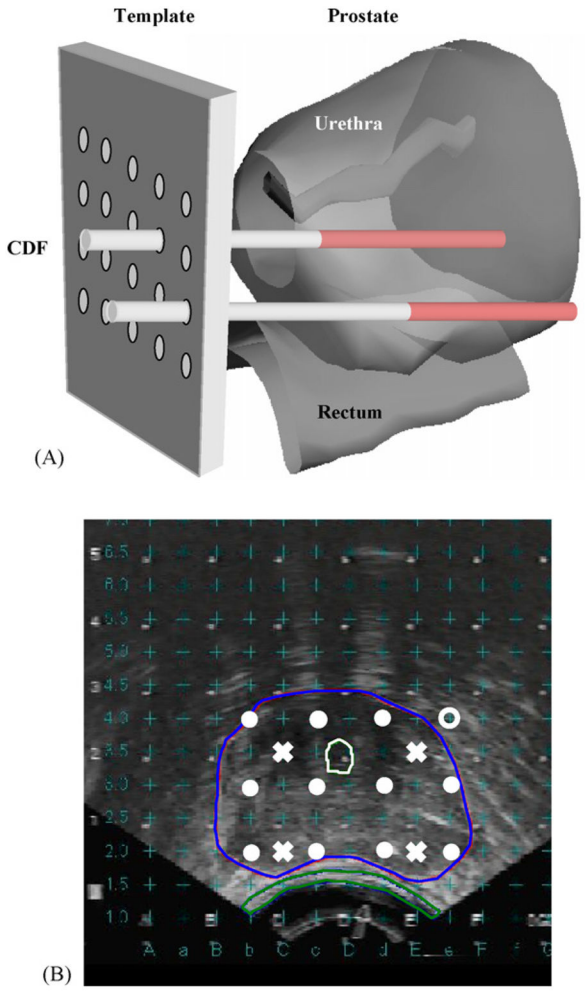

Figure 2.

(A) Schematic illustration of the prostate and surrounding anatomy and its relationship to the template used for the placement of catheters into the prostate. For simplicity, only two catheters are shown, with their active regions shaded and (B) typical transverse ultra-sounds image of a human prostate. The 0.5 cm by 0.5 cm grid of possible catheter locations is superimposed on the image. The locations of the light sources (filled circles) and detectors ('x' symbols) are indicated (taken from Ref. [72]).

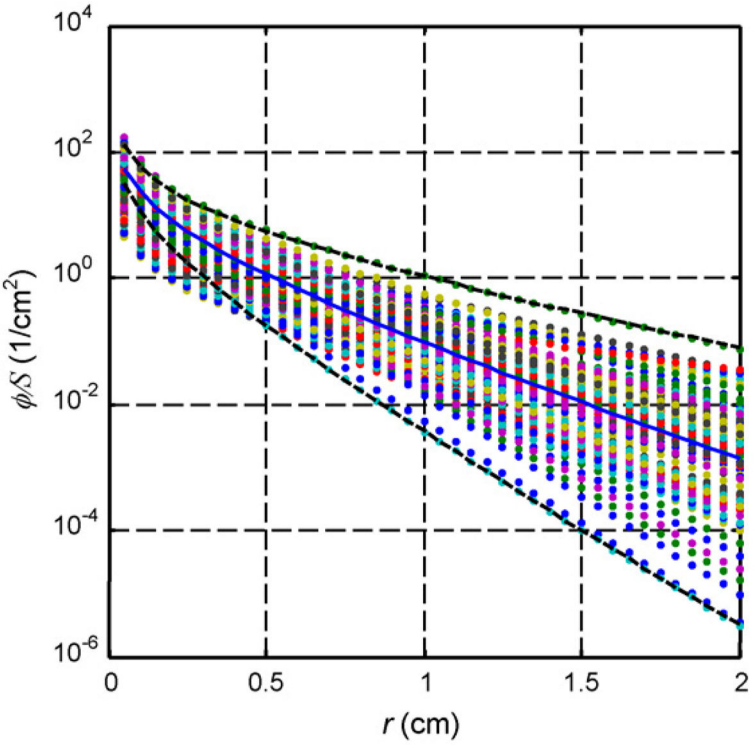

Figure 3.

Light fluence rate per source strength, φ/S, for a point source for the optical properties determined from human prostate. The solid line corresponds to φ/S for the average optical properties: μ_a = 0.3 cm^{-1}, $\mu_s^{'}$=14 cm^{-1}. The dashed lines corresponding to φ/S for the longest and shortest light penetrations: μ_a = 0.04 cm^{-1}, $\mu_s^{'}$=30 cm^{-1} and μ_a = 1.5 cm^{-1}, $\mu_s^{'}$=9 cm^{-1}, respectively (taken from Ref. [58]).

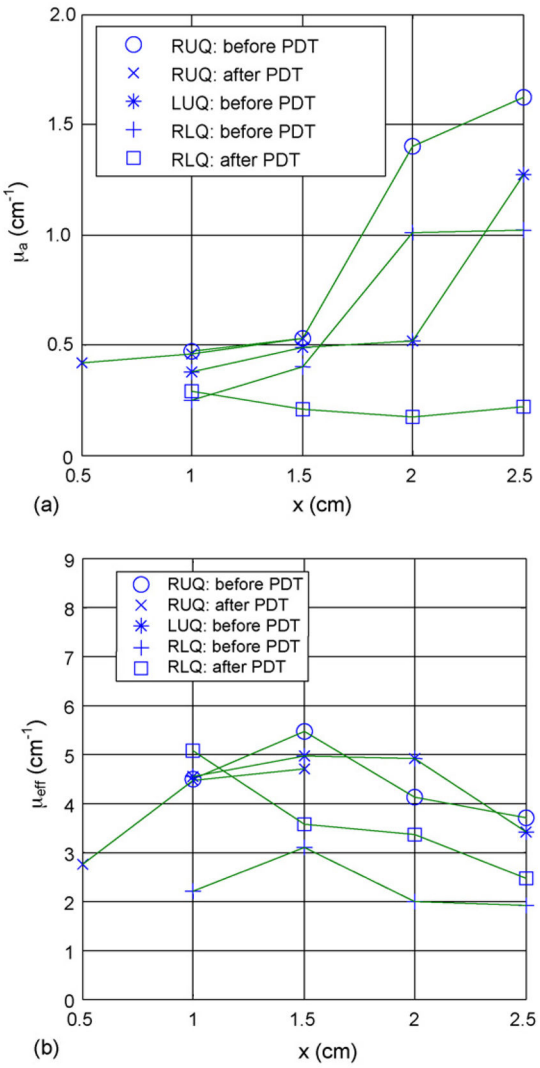

Figure 4.

In vivo distribution of (a) absorption and (b) effective attenuation coefficients at 732nm in the human prostate for patient #12. RUQ: right upper quadrant; LUQ: left upper quadrant; RLQ: left lower quadrant (taken from Ref. [58]).

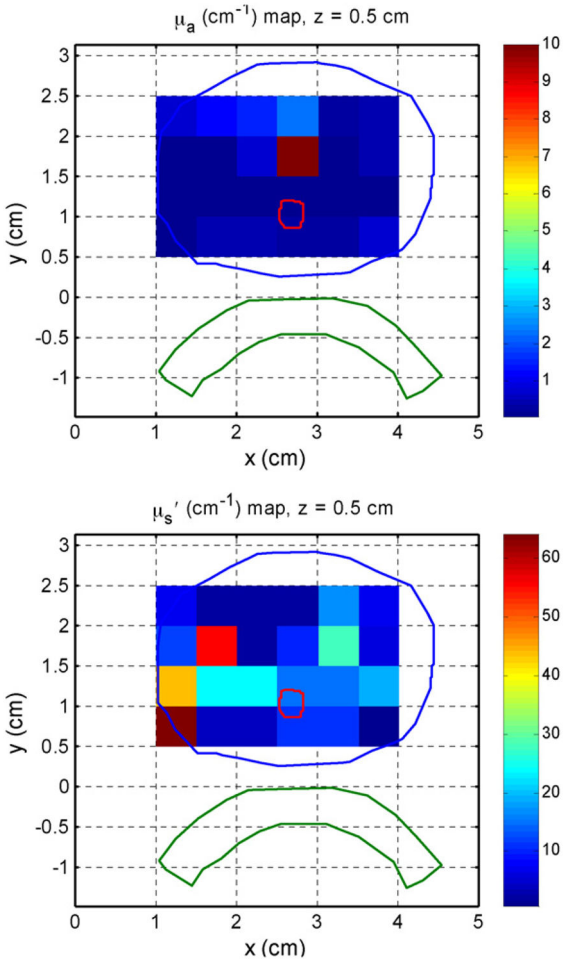

Figure 5.

3D reconstructed optical properties ((a) μ_a and (b) μ_s') at 732nm in human prostate before MLu-mediated PDT. The data was taken point-by-point for each 5×5mm^2 pixel, each assuming homogeneous optical properties within the pixel. See text for more details.

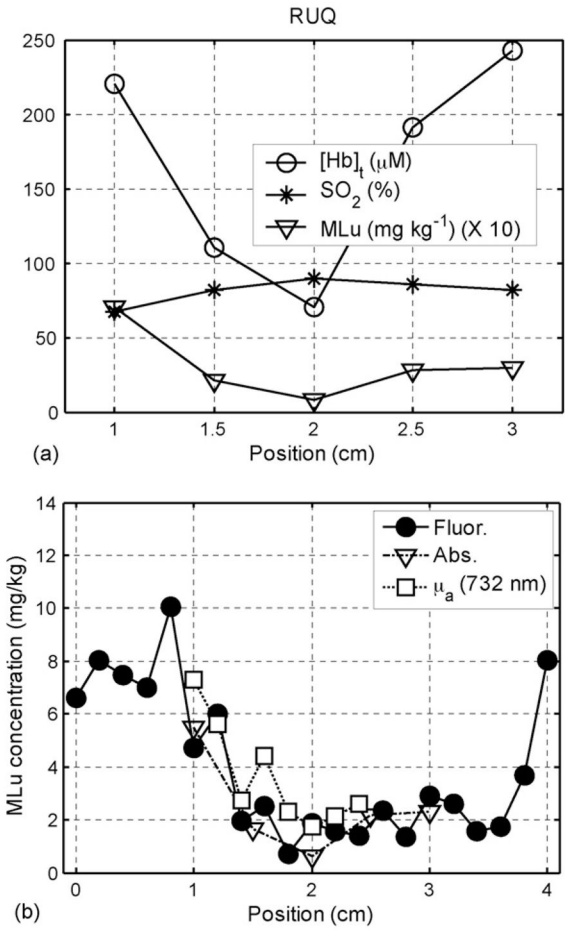

Figure 6.

In vivo distributions of (a) hemoglobin oxygenation (StO_2), blood volume, and MLu concentration determined using absorption spectroscopy in a typical human prostate prior to PDT and (b) MLu concentration as determined by absorption spectroscopy (triangles), 732-nm absorption measurements (squares), and fluorescence spectroscopy (circles) measurements. Both panels are taken from the RUQ in patient 13 (taken from Ref. [58]).

Table 1

List of photosensitizers currently or potentially undergoing human clinical trials for prostate cancer

Photosensitizer (trade name)	Approval	Excitation (nm)	Drug-light interval	Clearance time	Prostate status	Other sites
Porfimer sodium (Photofrin)	1998, 2003 (FDA)	630	48–150 h	4–6 weeks	Preclinical [12–14,76–78]	Various [79–83]
ALA-PpIX (Levulan)	1999 (FDA)	405, 635	14–18 h	~2 days	Clinical trial [6]	Various [84–92]
Methyl ALA-PpIX (Metvix)	2004 (FDA)	405, 635	3 h	~2 days		AK [93,94], NBCC [95]
Hexyl ALA-PpIX (Hexvix)	2005 (EU)	405	1–3 h	~2 days		Detection of bladder tumors
BPD-MA (Verteporfin, Visudyne)	2000 (FDA)	689	15 min	5 days	Preclinical [47,48]	Skin [96], AMD [97]
mTHPC (Foscan)	2001 (EU)	652	48–110 h	15 days	Clinical trial [5]	Various [98–100]
Motexafin Lutetium (MLu)	Phase I trials	732	3 h	~2 days	Clinical trial [7,8]	Various [101–103]
Pd-bacteriopheophorbide (Tookad)	Phase I & II trials	762	~6–15 min	~2 h	Clinical trial [9,10]	
Taloporfin Sodium (LS-11)	Phase I & II trials	664	1 h		*	Solid tumors [103]
Silicon pthalocyanine 4 (PC-4)	Phase I trials	672	24–36 h		*	

* Published results of preclinical and clinical trials are not yet available for these photosensitizers.